

The Effect of Schmidt Number on Air-Water Interface Mass Transfer

Y. Hasegawa and N. Kasagi

Department of Mechanical Engineering, The University of Tokyo
Hongo 7-3-1 Bunkyo-ku, Tokyo 113-8656, Japan
E-mail: hasegawa@thtlab.t.u-tokyo.ac.jp

ABSTRACT

The mass transfer across an air-water interface, specifically, the exchange of carbon dioxide between the atmosphere and the sea surface, was investigated by direct numerical simulation (DNS). As the Schmidt number of carbon dioxide in the seawater is known to be very high (~ 700), we have employed a Lagrangian approach, which has been successfully applied to the passive scalar transfer in DNS of turbulent channel flow. The result obtained by this method shows good agreement with the Eulerian DNS data at a low Schmidt number ($Sc = 1.0$) and also with experimental data at high Schmidt numbers ($Sc = 100, 500, 1000$).

Although the eddy diffusivity near a wall is decreased as increasing the Schmidt number, it does not largely depend on the Schmidt number at a free surface. This suggests that the correlation between velocity and concentration fields near a free surface is kept unchanged even at a very high Schmidt number at a free surface

INTRODUCTION

The gas transfer across an air-water interface is a very important phenomenon in various engineering and environmental problems, such as, the physical process of chemical reactors, and the exchange of slightly soluble gasses like O_2 or CO_2 between the atmosphere and the oceans. Since the concentration boundary layer in the liquid phase is very thin for such gases, it is important to investigate the fine-scale turbulence structure and associated concentration field in the vicinity of the interface in order to explore the detailed mechanism of gas transfer at the air-water interface. However, the measurement of instantaneous velocity and concentration fluctuations near an interface is extremely difficult and the accuracy of experimental data available is in many cases unsatisfactory.

Recently, direct numerical simulation of open channel flow has been carried out by several groups [1, 2, 3] and they have shown the advantage of DNS in clarifying the complex mechanism of mass trans-

fer. In these pieces of work, it is found that the vortices generated at the bottom wall migrate to the free surface, and that such quasi-streamwise vortices play an important role in the interfacial mass transfer across the free-surface.

Most of these simulations have dealt with the liquid side turbulence without no wind shear. Considering real ocean surfaces, the interaction between gas and liquid turbulent fields is not negligible, especially, for slightly soluble gases. Lombardi *et al.* [1] have carried out DNS, in which the gas and liquid sides are coupled each other without complexity of interface deformation.

In the present study, we also employ a DNS code, with two fluid domains coupled through the continuity of velocity and shear stress, to study the mechanism of mass transfer across the interface. Although DNS is a powerful tool to investigate the fine-scale turbulence near the interface, the computational load would be too large for Schmidt numbers as high as those of O_2 or CO_2 in oceans or lakes. This is because the number of grids required to capture the smallest scale of concentration field becomes unrealistically large. Therefore, in almost all the DNS of free-surface turbulence, the Schmidt number has been limited to the order of unity.

Recently, Na *et al.* [4] have applied a Lagrangian method, in which the mean concentration is calculated by the probability density function of particle migration from a point source, to the passive scalar transfer in turbulent channel flow. Their result is in good agreement with the Eulerian DNS data at low Schmidt numbers and also with the experimental data for high Schmidt numbers.

Presently, the fully developed turbulence near an interface between two flowing fluids is investigated numerically to study the effect of Schmidt number on the mass transfer. For high Schmidt numbers ($Sc = 100, 500, 1000$), the Lagrangian method is employed. Comparison between scalar transfer near a

wall and a free surface is also made.

NUMERICAL METHOD

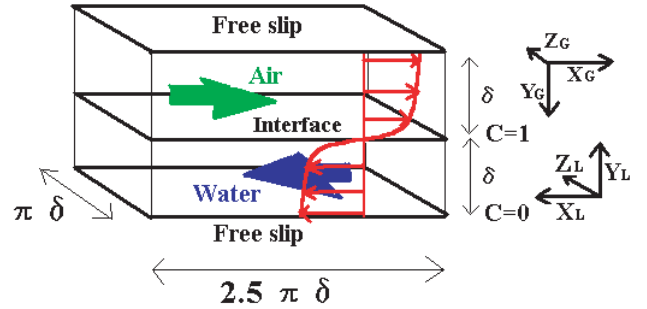


Fig. 1 Computational domain and coordinate system

In Fig. 1 the computational domain is shown. The depth of both subdomains is δ , and their horizontal dimensions are $2.5\pi\delta$ and $\pi\delta$ in the streamwise and spanwise directions. Periodic boundary conditions in the streamwise and spanwise directions are imposed in each subdomain. The Reynolds number ($Re_\tau = u_\tau\delta/\nu$), which is based on the depth of each domain δ , the friction velocity at the interface u_τ , and the kinematic viscosity ν , is 150 in both the liquid and gas phases. The density ratio of the two fluids is $\rho_L/\rho_G = 841$, which corresponds to air and water at atmospheric pressure and about 320K.

Free-shear boundary conditions are applied at the outer edge of each subdomain. At the interface of two subdomains, continuity of the velocity, shear stress, scalar concentration and scalar flux are imposed. The effect of interface deformation is not discussed because the experimental data of Komori *et al.* [5] and the DNS of De Angelis and Banerjee [6] showed that the effect of deformation on turbulent field and mass transfer is negligible in a low-Reynolds number turbulence as in this study.

The governing equations for an incompressible Newtonian fluid and its scalar field, *i.e.*, the continuity, Navier-Stokes, and scalar transport equations, are given as:

$$\frac{\partial u_i}{\partial x_i} = 0 \quad (1a)$$

$$\frac{\partial u_i}{\partial t} + u_j \frac{\partial u_i}{\partial x_j} = -\frac{\partial p}{\partial x_i} + \frac{1}{Re} \frac{\partial^2 u_i}{\partial x_j \partial x_j} \quad (1b)$$

$$\frac{\partial C}{\partial t} + u_j \frac{\partial C}{\partial x_j} = \frac{1}{Re Sc} \frac{\partial^2 C}{\partial x_j \partial x_j} \quad (1c)$$

The pseudospectral method is used to discretize the above equations in each domain. Fourier expansions are employed in the streamwise, x , and spanwise, z , directions, while Chebyshev expansion in the y direction normal to the interface. The time advancement is made by the second-order Adams-Bashforth scheme for the convective terms and by the Crank-Nikolson method for the viscous terms. The simulation is carried out on a $64 \times 48 \times 64$ grid in each subdomain.

In order to satisfy the condition of shear stress and velocity continuity at the interface, the fractional time step method is used. For the first half time step, one subdomain (the gas phase) is solved imposing only continuity of the velocity at the interface, and then for the second half time step, the other subdomain (the liquid phase) is solved imposing continuity of the shear stress. The details of the numerical algorithm is found in Lombardi *et al.* [3].

In Fig. 2, the time-mean concentration profile obtained by the Eulerian method is shown. In this case, the Schmidt numbers in both subdomains are 1.0. The distance in the direction normal to the interface y is nondimensionalized by the depth of the subdomain δ , whilst the scalar field is nondimensionalized by the concentration difference between two outer edges of subdomains, ΔC . Although the Schmidt numbers are the same ($Sc_G = Sc_L = 1.0$), the most of concentration change occurs on the liquid side. From this result, it is expected that the resistance to the mass transfer at an interface is much larger in the liquid phase than in the gas phase.

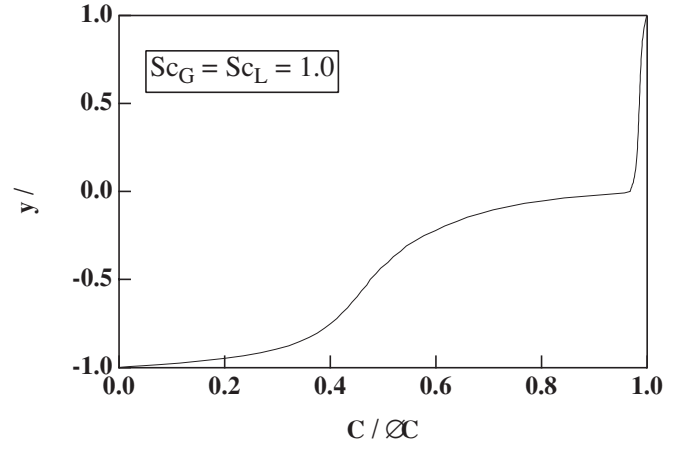


Fig. 2 Profile of time-mean concentration

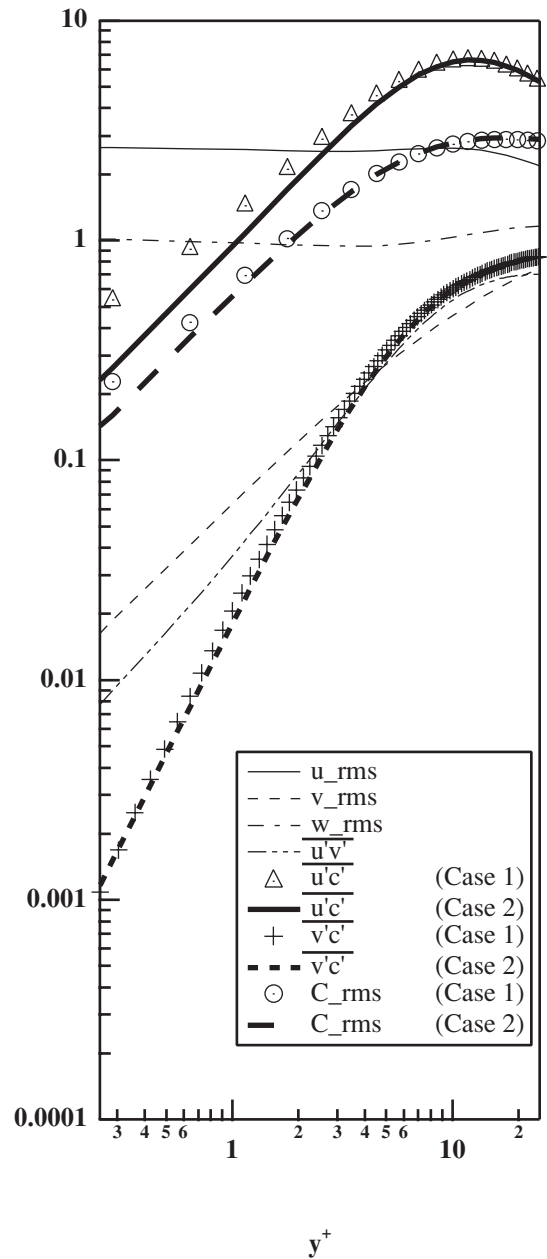


Fig. 3 Limiting behavior of turbulent statistics near the interface

In Fig. 3, the limiting behavior of turbulent statistics near the interface in the liquid phase is shown. In Case 1 the concentration fields are solved in both the gas and liquid phases, but in Case 2 only the concentration field of the liquid phase is solved with the constant concentration condition imposed at the interface. The latter adhoc assumption is intended to reduce the computational load. The distance from the interface y^+ is nondimensionalized by the liquid-phase friction velocity at the interface u_τ and the kinematic viscosity ν . Within $y^+ < 1.0$, the effect of the different boundary conditions on the concentration fluctuation C_{rms} and turbulent scalar flux $\overline{u'c'}$ is discernible, but another scalar flux $\overline{v'c'}$ normal to the interface is unchanged. Therefore, this difference of the scalar boundary condition hardly affects the mean concentration profile and the mass transfer rate. As a result, it can be said that the constant concentration condition is satisfied at the interface in the case of low Schmidt numbers.

With increasing the Schmidt number in the liquid phase, the resistance to the absorption is more dominated by the liquid side, and if so, the constant concentration condition at the interface can be verified for investigating the liquid side transfer mechanism. From this result, we presently assume the constant concentration at the interface for high Schmidt numbers, and solve only the liquid side concentration, although we solve the coupled velocity fields for both sides. Imposing this assumption, the comparison between scalar transfer near a wall and a free surface at the constant scalar boundary condition is also made.

LAGRANGIAN METHOD

The Lagrangian method developed by Papavassiliou and Hanratty [7] has been applied to a passive scalar transfer at high Schmidt numbers in DNS of turbulent channel flow [4]. Calculating the

concentration fields at high Schmidt numbers by the Eulerian method is very limited because the number of grid points required to capture the smallest scalar scale increases. In Lagrangian method the trajectories of scalar markers released at the initial time t_0 from a point source are calculated in DNS.

Each marker moves due to convective and molecular effects. The convective effect is calculated from a fluid velocity at the marker's location. The effect of molecular motion is simulated by imposing a three-dimensional random walk on the particle motion and it is added to the convective motion at each time step. The magnitude of random walk is calculated from a Gaussian distribution with zero mean and standard deviation σ , which is given by the time step Δt and the Schmidt number as flows:

$$\sigma = \sqrt{\frac{2}{Sc} \Delta t} \quad (2)$$

Sample particle trajectories are used for calculating the probability density function (PDF) of $P(x-x_0, y, z-z_0; t-t_0)$ where presents the ensemble average of markers released instantaneously from a point source. The distribution of the mean concentration over a plane source is calculated by integrating the probability function P over time and plane as:

$$\bar{P}(y) = \int_{t_0}^{\infty} \int_{z_0}^{\infty} \int_{x_0}^{\infty} P(x-x_0, y, z-z_0; t) dx dz dt \quad (3)$$

Applying the Lagrangian approach, the calculations can be performed for Sc much higher than in the Eulerian method. However, in the Lagrangian method, it is necessary to prepare sufficiently fine grids for accurately obtaining a steep distribution of temperature field in the vicinity of the boundary. The details on this point are found in Papavassiliou and Hanratty [7].

LAGRANGIAN SIMULATION OF CHANNEL FLOW

To compare the effect of Schmidt number on the mass transfer in wall turbulence and free surface turbulence, passive scalar transfer in fully developed turbulent channel flow is calculated at high Schmidt numbers ($Sc = 100, 500, 1000$) by mean of the Lagrangian method. The calculation is done with a $128 \times 64 \times 128$ grid. Cubic spline fitting is used for interpolating Eulerian velocity grid data. The details of particle tracking method can be found in Mizuya and Kasagi [8], and Kontomaris and Hanratty [9]. The Reynolds number based on the half height of the channel and the friction velocity is 150. Constant concentration conditions are imposed at both walls. 160,000 markers are released from a 400×400 grid that covers the bottom wall.

In Fig. 4, the Lagrangian and Eulerian results for $Sc = 0.1$ and 0.71 are compared. They show very good agreement. The Lagrangian results of mean concentration distributions at high Schmidt numbers are shown in Fig. 5. In these cases ($Sc = 100, 500, 1000$), the conductive sublayer remains in the region of $y^+ < 1.0$, and the most concentration change occurs in the region of $y^+ < 10$.

With the Schmidt number increased, the concentration boundary layer becomes so thin that the turbulent structure in the immediate vicinity of the wall governs the mass transfer. To study the turbulent velocity and concentration fields near the wall, the limiting behavior is discussed below. If the fluctuating velocity and concentration fields are expanded in Taylor series, the following equations are obtained for a given Schmidt number:

$$u(x, y, z, t) = \alpha_1(x, z, t) \cdot y + \alpha_2(x, z, t) \cdot y^2 + \dots \quad (4a)$$

$$v(x, y, z, t) = \beta_2(x, z, t) \cdot y^2 + \beta_3(x, z, t) \cdot y^3 + \dots \quad (4b)$$

$$u(x, y, z, t) = \gamma_1(x, z, t) \cdot y + \gamma_2(x, z, t) \cdot y^2 + \dots \quad (4c)$$

$$c(x, y, z, t) = c_1(x, z, t) \cdot y + c_3(x, z, t) \cdot y^3 + \dots \quad (4d)$$

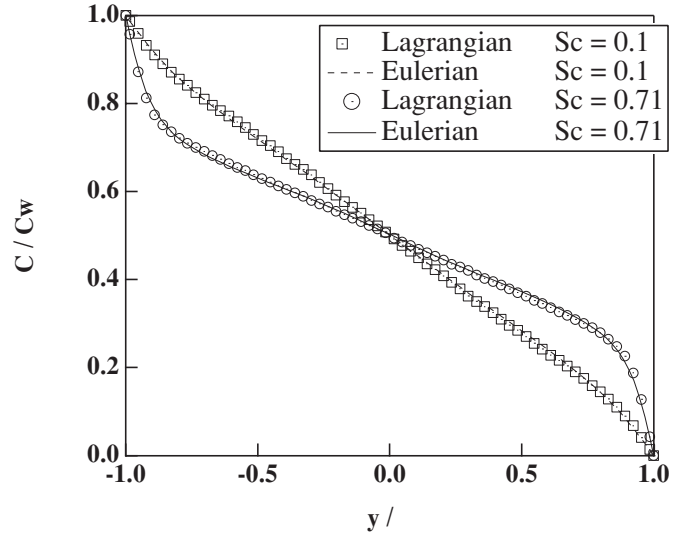


Fig. 4 Mean concentration at low Schmidt numbers

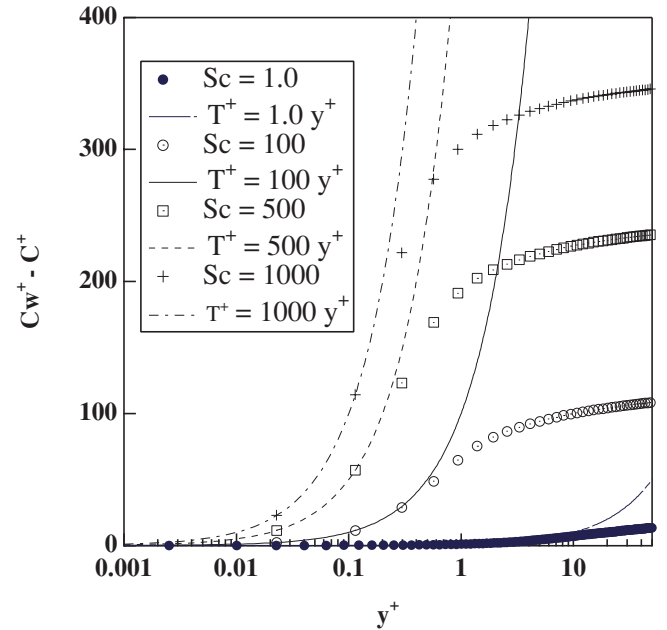


Fig. 5 Mean concentration at high Schmidt numbers

$$\overline{uv} = \overline{\alpha_1 \beta_2} \cdot y^3 + \overline{\alpha_1 \beta_3 + \alpha_2 \beta_2} \cdot y^4 + \dots \quad (4e)$$

$$\overline{cv} = \overline{c_1 \beta_2} \cdot y^3 + \overline{c_1 \beta_3} \cdot y^4 + \dots \quad (4f)$$

Because of the continuity condition at a no-slip and non-permeable wall, the velocity fluctuation normal to the wall varies quadratically with the distance from the boundary. The nondimensionalized eddy diffusivities for momentum and scalar, can be expanded in the same manner. If we consider only the first term of Taylor series for the vicinity of the wall, the nondimensionalized eddy diffusivity for momentum Ev^+ and eddy diffusivity for scalar Ec^+ , are given as flows:

$$Ev^+ = \overline{\alpha_1 \beta_2} \cdot y^3 \quad (5a)$$

$$Ec^+ = \frac{\overline{c_1 \beta_2}}{Sc} \cdot y^3 \quad (5b)$$

The analogy between momentum and scalar transfer requires Ec^+ varying as y^{+3} and the proportionality constant which is independent of the Schmidt number. This analogy has been widely used for predicting heat or scalar transfer in wall turbulence. Using this analogy, the averaged scalar transfer equation is given as flows:

$$1 = -\left(\frac{1}{Sc} + Ec^+\right) \frac{d\bar{C}}{dy} = -\left(\frac{1}{Sc} + A \cdot y^3\right) \frac{d\bar{C}}{dy} \quad (6a)$$

$$A = \frac{\overline{c_1 \beta_2}}{Sc} = const \quad (6b)$$

This averaged scalar transport equation gives the nondimensionalized mass transfer rate, $K^+ = K/u_\tau$, which is proportional to $Sc^{-2/3}$.

In Fig. 6, the limiting behavior of the eddy diffusivities for scalar Ec^+ for $Sc = 1.0$ by the Eulerian method and at high Schmidt numbers by the Lagrangian method is shown. The eddy diffusivity for momentum Ev^+ is also presented. The two kinds of eddy diffusivities become the same at $Sc = 1.0$, because the complete analogy of governing equations and boundary conditions for the velocity and scalar fields is satisfied.

With the Schmidt number increased, the eddy diffusivity for scalar decreases in the vicinity of the wall. It means the analogy between the momentum and scalar transfer does not hold in turbulent channel flow. This result agrees with Na *et al.* [4, 10], who performed DNS of passive scalar transfer in fully developed turbulent channel flow for Schmidt numbers up to 10. From these results, it is concluded that the mass transfer rate would not be exactly proportional to $Sc^{-2/3}$ for very high Schmidt numbers.

The mass transfer rate, K^+ , is represented as a function of Sc in Fig. 7. The symbols are results from

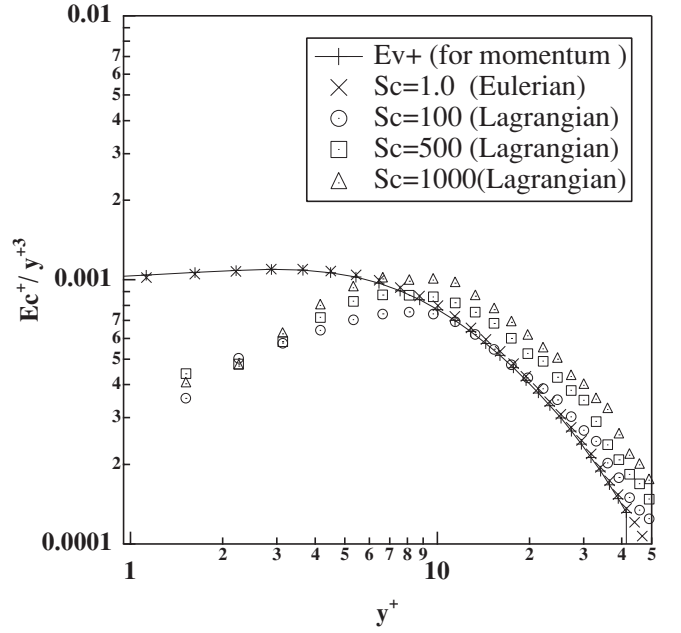


Fig. 6 Limiting behavior of eddy diffusivities at different Schmidt number

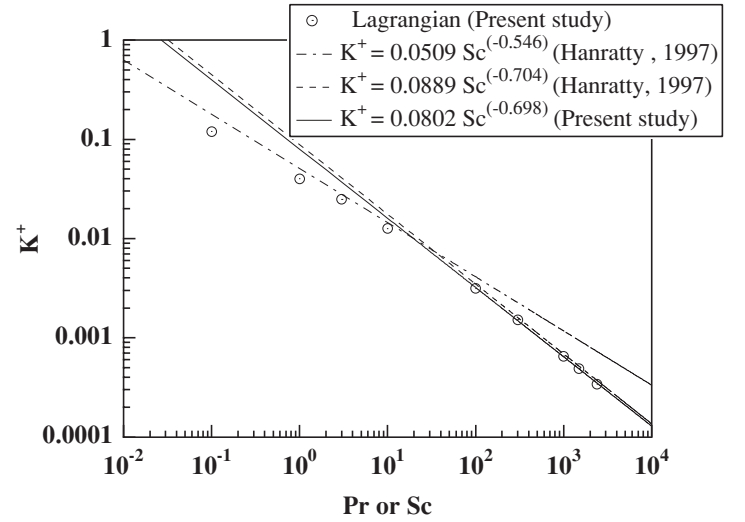


Fig. 7 Mass transfer rate as a function of Pr or Sc

the present study of the Lagrangian method and the broken line represents the relation by Shaw and Hanratty [11] from their measurements of mass transfer in a pipe over a range of Schmidt numbers of 693 to 39,300. The dash-dotted line represents the relation from the DNS at low Schmidt numbers by Na *et al.* [4]. The mass transfer rate from the present study is proportional to $Sc^{-0.698}$ for high Sc numbers (the solid line), and this fact is consistent with the calculations by Na *et al.* [4], but contradictory to the clas-

sical theory based on the analogy between momentum and scalar transfer.

LAGRANGIAN SIMULATION OF GAS-LIQUID TURBULENCE

According to the discussion in the preceding section, the analogy between momentum and scalar transfer is not satisfied in wall turbulence at high Schmidt numbers, and the proportional constant of eddy diffusivity largely depends on the Schmidt number. Therefore, it is of interest to know whether these same conclusions are applicable to sheared, air-water interfaces.

To study the mass transfer at high Schmidt numbers ($Sc = 100, 500, 1000$), the Lagrangian method is applied to a DNS of the gas-liquid turbulence. The domain geometry and the numerical schemes for the velocity field and particle tracking are the same as described. We impose constant concentration condition at an interface, and only solved the concentration field in the liquid phase.

In Fig. 8, the profiles of mean concentration are shown. The concentration boundary layers at a free surface are almost ten times thinner than those at a wall at the same Schmidt numbers. It is reflecting the fact that for this range of Schmidt numbers, the mass transfer rates at a free surface are about ten times larger than those at a wall (see, Figs. 7 and 10).

Equations (4a-f) of the limiting behavior of turbulent quantities for a wall are modified for a free surface as follows:

$$u(x, y, z, t) = \alpha_0(x, z, t) + \alpha_1(x, z, t) \cdot y + \dots \quad (7a)$$

$$v(x, y, z, t) = \beta_1(x, z, t) \cdot y + \beta_2(x, z, t) \cdot y^2 + \dots \quad (7b)$$

$$w(x, y, z, t) = \gamma_0(x, z, t) + \gamma_1(x, z, t) \cdot y + \dots \quad (7c)$$

$$c(x, y, z, t) = c_1(x, z, t) \cdot y + c_2(x, z, t) \cdot y^2 + \dots \quad (7d)$$

$$\overline{uv} = \overline{\alpha_0\beta_1} \cdot y + \overline{(\alpha_0\beta_2 + \alpha_1\beta_1)} \cdot y^2 + \dots \quad (7e)$$

$$\overline{cv} = \overline{c_1\beta_1} \cdot y^2 + \overline{(c_1\beta_2 + c_2\beta_1)} \cdot y^3 + \dots \quad (7f)$$

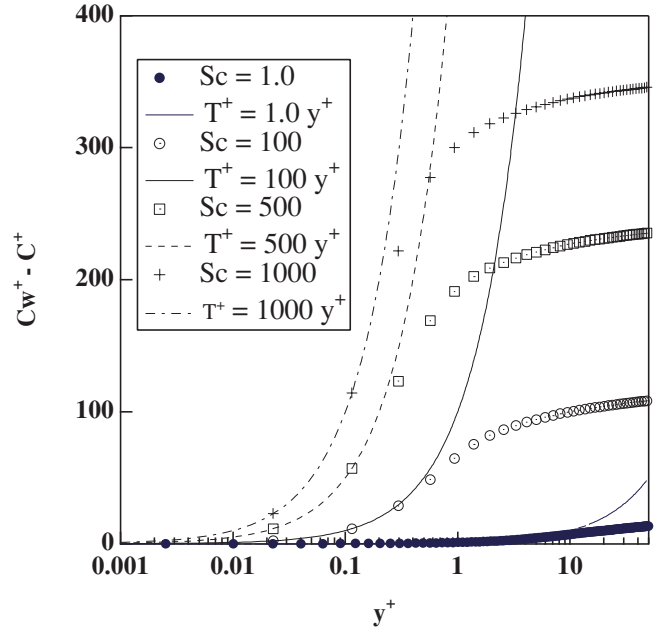


Fig. 8 Mean concentration near the air-water interface

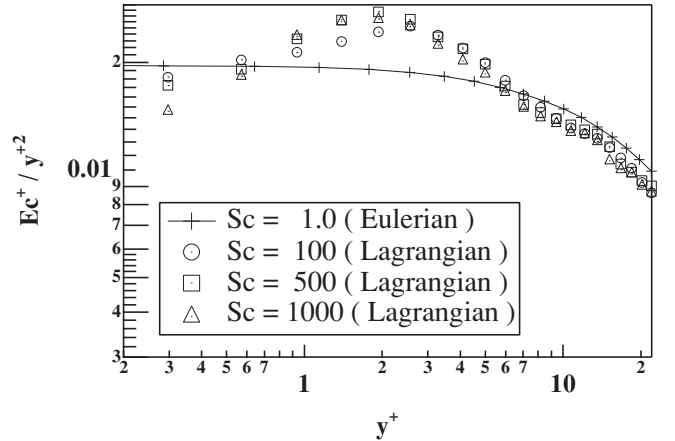


Fig. 9 Limiting behavior of eddy diffusivities near the air-water interface

Since the fluid velocity has a non-zero value at the interface, the velocity normal to the interface varies linearly rather than quadratically. If we take into account only the first term of Taylor series, the eddy diffusivities for momentum and scalar near the interface are represented as flows:

$$Ev^+ = \overline{\alpha_0\beta_1} \cdot y \quad (8a)$$

$$Ec^+ = \frac{\overline{c_1\beta_1}}{Sc} \cdot y^2 \quad (8b)$$

where the limiting behavior of eddy diffusivity for momentum is different from that of eddy diffusivity for scalar. Thus, the analogy between momentum and scalar transfer does not hold in the vicinity of the

interface.

Figure 9 shows the limiting behavior of eddy diffusivity for scalar for a low Schmidt number ($Sc=1.0$) by the Eulerian method and those at high Schmidt numbers ($Sc=100, 500, 1000$) by the Lagrangian method. With increasing the Schmidt number, the value of eddy diffusivity for scalar slightly decreases near the interface. However, the results do not show strong dependence on the Schmidt number unlike the results in Fig. 6. The limiting behavior of eddy diffusivity in the conductive sublayer ($y^+ < 0.1$) could not be obtained, because in the Lagrangian method, the eddy diffusivity is calculated from the profile of the mean concentration instead of direct measurements of Reynolds transport [10]. However, the eddy diffusivity in the conductive sublayer does not affect mean concentration profile and mass transfer rate. Therefore, the eddy diffusivity for scalar, $Ec^+ \propto y^{+2}$, as well as the proportionality constant is independent of the Schmidt number, are confirmed in the vicinity of the interface. It is deduced that the mass transfer rates are proportional to $Sc^{-0.5}$ for high Schmidt numbers at a free surface.

In Fig. 10, the mass transfer rates are represented as a function of the Schmidt numbers. The experimental data for high Schmidt numbers have been compiled by Hanratty [12] as:

$$K^+ = \frac{K_L}{u_\tau} = 0.12 \sim 0.15 \cdot Sc^{-0.5} \quad (9)$$

De Angelis and Banerjee [6] performed DNS of a passive scalar in a coupled gas-liquid turbulence for Schmidt number up to 100. They also obtained the relation between the mass transfer and the Schmidt number as:

$$K^+ = \frac{K_L}{u_\tau} = 0.108 \sim 0.158 \cdot Sc^{-0.5} \quad (10)$$

Calmet and Magnaudet [13] carried out a Large Eddy Simulation of a free surface turbulence for $Re_\tau=1280$ and $Sc = 200$. These data are also plotted in Fig.10

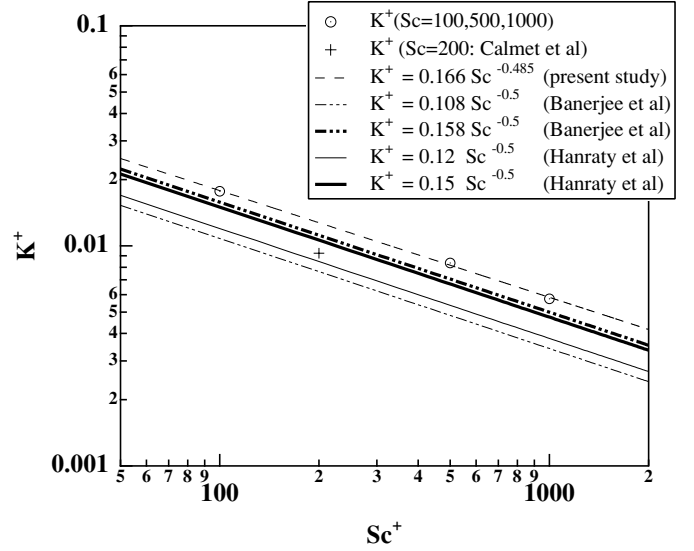


Fig. 10 Mass transfer rate as a function of Schmidt number at the air-water interface

for comparison.

Although the present condition of the calculation is different in the Reynolds number and the boundary condition, the results obtained agree well with the previous results. The classical theory can be applied to a gas-liquid interface, and the mass transfer rate is proportional to $Sc^{-0.5}$ even at high Schmidt numbers.

VISUALIZATION OF TURBULENCE STRUCTURES

To study the relationship between turbulent structures and mass transfer, flow visualization was performed with a conditional sampling method based on particle locations. A total of 1000 particles were released from a wall and also from an interface. If a particle passes through a prescribed horizontal plane ($x-z$ plane) located at a certain distance from a wall or an interface, the flow field around the particle was sampled and ensemble average of the samples was calculated in order to clarify the vortex structures which contribute to the mass transfer.

The Schmidt numbers of particles were assumed as $Sc = 100$ in both wall turbulence and free

surface turbulence. In the case of gas-liquid turbulence, the x - z planes for sampling particles were located at $y^+ = 0.3, 1.15,$ and $1.78,$ which correspond to

inside the sublayer, the middle of concentration boundary layer, the outer concentration boundary layer, respectively. In the case of wall turbulence, the

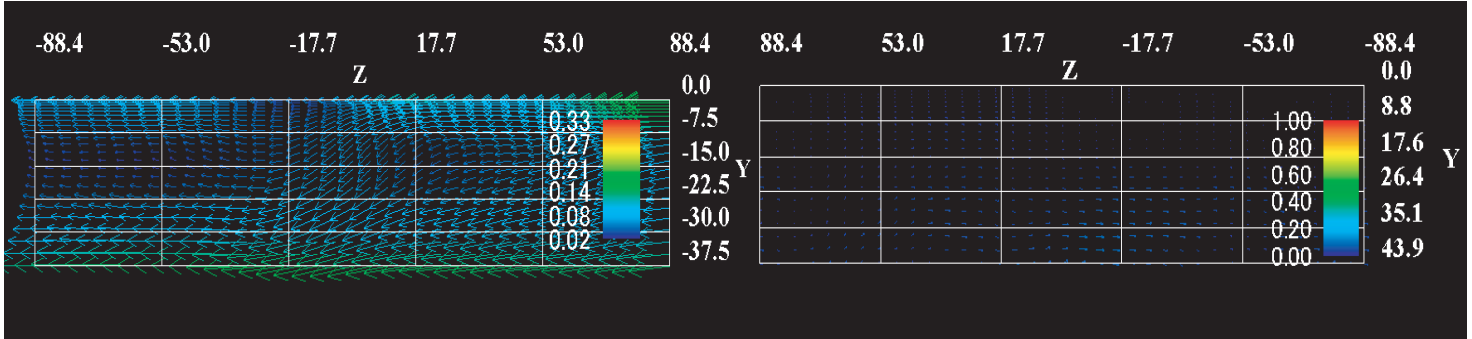


Fig.11 Ensemble-averaged velocity field around a marker which passes $y^+ = 0.3$ plane from the air-water interface

Fig.14 Ensemble-averaged velocity field around a marker which passes $y^+ = 1.0$ plane from the wall

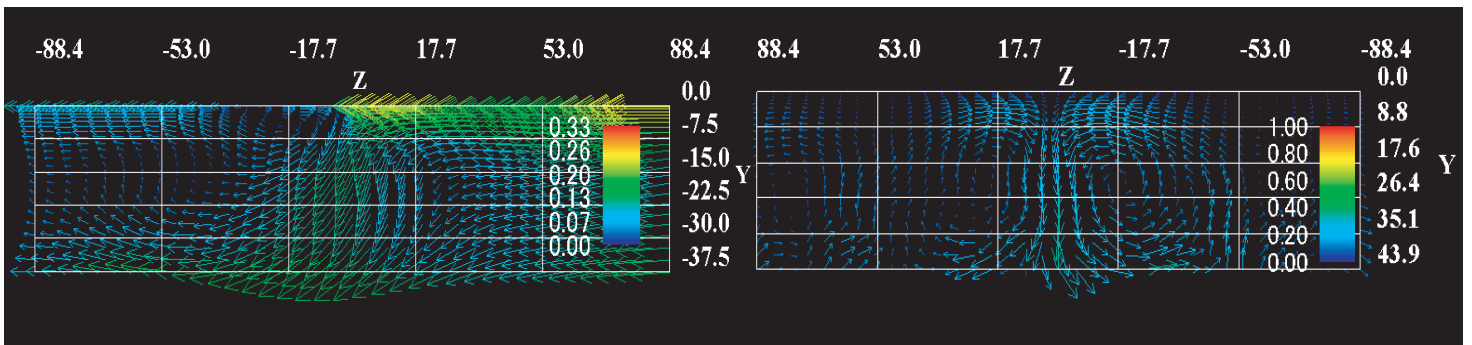


Fig.12 Ensemble-averaged velocity field around a marker which passes $y^+ = 0.65$ plane from the air-water interface

Fig.15 Ensemble-averaged velocity field around a marker which passes $y^+ = 5.0$ plane from the wall

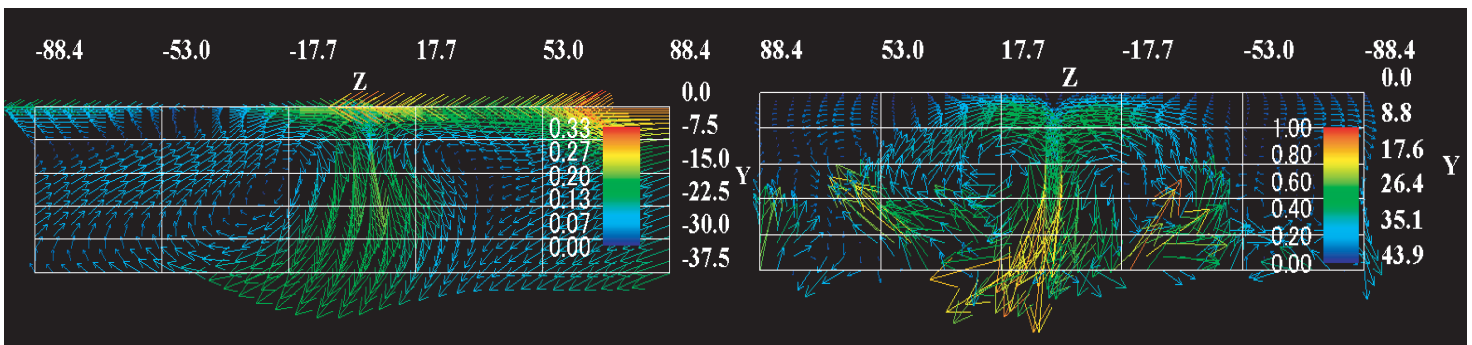


Fig.13 Ensemble-averaged velocity field around a marker which passes $y^+ = 1.78$ plane from the air-water interface

Fig.16 Ensemble-averaged velocity field around a marker which passes $y^+ = 10.0$ plane from the wall

x - z planes for conditioning were located at $y^+ = 1.0$, 5.0, and 10.0.

In Figs. 11, 12, and 13, the ensemble-averaged flow fields in the y - z plane (normal to the streamwise direction) around sampled markers are shown for gas-liquid turbulence. At $y^+=0.3$, this region is located inside the conductive sublayer (see Fig. 8), so that the mass transfer is mainly governed by the molecular diffusion rather than turbulent transport. As increasing the distance from the interface, a pair of streamwise vortex structures appears beneath an interface, which is identified to play an important role in transferring scalar.

In Figs. 14, 15, and 16, the ensemble-averaged flow fields in the turbulent channel flow are shown. Like in the gas-liquid flow, as increasing the distance from the wall, the streamwise vortex structure appears more clearly in the vicinity of the wall. In wall turbulence, however, the effect of vortex structure on the mass transfer is rapidly decreasing as approaching to the wall, because the no-slip condition is imposed at the wall (see Fig. 14). On the other hand, in the gas-liquid flow, the vortex structure beneath the interface generates strong horizontal velocity fluctuations near the interface, which certainly generates strong velocity fluctuations normal to the interface. This velocity fluctuation normal to the interface should play an important role in transferring scalar in the vicinity of an interface, especially at high Schmidt numbers. Therefore, the high Schmidt number mass transfer is prompted more in gas-liquid turbulence than in wall turbulence.

CONCLUSIONS

Direct numerical simulation of the coupled gas-liquid turbulent flow was carried out. With the Lagrangian method, the mean concentration profiles and mass transfer rates at high Schmidt numbers were calculated. The results obtained in the present study

agree well with the previous experimental and numerical data.

At a solid wall, the wall limiting value of eddy diffusivity for scalar is decreasing with the Schmidt number increased; this results in the fact that the analogy between momentum and scalar transport does not hold, so that the mass transfer rate is not exactly proportional to $Sc^{-2/3}$. On the other hand, in the vicinity of a gas-liquid interface, the dependence of the limiting value of eddy diffusivity on the Schmidt number should be negligibly weak. Therefore, using the classical theory, the mass transfer rates are proportional to $Sc^{-0.5}$ even at high Schmidt numbers.

From the visualization of ensemble-averaged flow fields, it is confirmed that the streamwise vortex structures induce the velocity fluctuations even in the close vicinity of the gas-liquid interface. This fact explains why the mass transfer rates at a gas-liquid interface are much larger than those at a solid wall for high Schmidt numbers.

ACKNOWLEDGMENTS

The authors are grateful to Professor Hideshi Hanazaki at Tohoku University for his useful discussions and encouragement during the course of this work.

REFERENCES

1. Lombardi, P., De Angelis, V., and Banerjee, S., Direct numerical simulation of near -interface turbulence in coupled gas-liquid flow, *Phys. Fluids*, Vol. 8, No. 6, pp. 1643-1665, 1996.
2. Nagaosa, R., Direct numerical simulation of vortex structures and turbulent scalar transfer across a free surface in a fully developed turbulence, *Phys. Fluids*, Vol.11, No.6, pp. 2607-2625, 1999.
3. Handler, R. A., Saylor, J. R., Leighton, R. I., and Rovelstad A. L., Transport of a passive scalar at a shear-free boundary in fully developed turbulent channel flow, *Phys. Fluids*,

- Vol.11, No.9, pp. 2607-2625, 1999.
4. Na, Y., Papavassiliou, D., and Hanratty T. J., Use of direct numerical simulation to study the effect of Prandtl number on temperature fields, *Int. J. Heat and Mass transfer*, Vol. 20, pp. 187-195, 1999.
 5. Komori, S., Nagaosa, R., and Murakami, Y., Turbulent structure and mass transfer across a sheared air- water interface in wind-driven turbulence, *J. Fluid Mech.*, Vol. 249, pp. 161-183, 1993.
 6. De Angelis, V., and Banerjee, S., Heat and mass transfer mechanism at wavy gas-liquid interfaces, *TSEFP*, pp. 1249-1245, 1999.
 7. Papavassiliou, D., and Hanratty T. J., The use of Lagrangian method to describe turbulent transport of heat from a wall, *Ind. Eng. Chem. Res.*, Vol. 34, pp. 3359-3367, 1995.
 8. Mizuya, R., and Kasagi, N., Numerical analysis of particle motion in turbulent channel flow, Proc. 3rd. Int. Conf. Multiphase Flow, Lyon, in CD-ROM, P632.pdf, pp. 1-6, June 1998.
 9. Kontomaris, K., and T. J. Hanratty, An algorithm for tracking fluid particles in a spectral simulation of turbulent channel flow, *J. Comp. Phys.*, Vol. 103, pp. 231-242, 1992.
 10. Na, Y., and Hanratty T. J., Limiting behavior of turbulent scalar transport close to a wall, *Int. J. Heat and Mass transfer*, Vol. 43, pp. 1749-1758, 2000.
 11. Shaw, D. A., and Hanratty T. J., Turbulent mass transfer to a wall for large Schmidt numbers, *AIChE Journal*. Vol. 23, pp. 28-37, 1977.
 12. Hanratty, T. J., Effect of gas flow on physical absorption. In: Wilhelms, Gulliver (Eds.), Air-water gas transfer, ASCE (Civil Engineers), New York, 1991.
 13. Calmet, I., and Magnaudet J., High-Schmidt number mass transfer through gas-liquid interfaces, *Int. J. Heat and Fluid Flow*, Vol. 19, pp. 522-532, 1998.
 14. McCready, M. J., Vissiliadou, E., and Hanratty T. J. 'Computer simulation of turbulent mass transfer at a mobile interface', *AIChE Journal*, Vol. 32, No. 7, pp. 1108-1115, 1986.
 15. Fortescue, G. E. and Pearson, J. R. A., On gas absorption into a turbulent liquid. *Chem. Eng. Sci.*, Vol. 22, pp. 1163-1176, 1967.
 16. Komori, S., Ueda, H., Ogino, F. and Mizushima, T., *Int. J. Heat and Mass Transfer*, Vol.25, pp. 513-522, 1982.